Assessing land use and land cover changes from 1989 to 2021 in relation to economic zone construction along mangrove forests on the east coast of Bangladesh

Abstract

Coastal ecosystems, represented by mangrove forests, have been degraded by human activities, making ecosystem restoration essential to reinstate ecosystem services. Since 2016, a governmental program has led to the exploitation of mangroves along the eastern coast of Bangladesh. To assess the impacts, land use and land cover (LULC) changes were monitored before and after the exploitation, from 1989 to 2021, covering 192 km^2 of mangrove plantation and surrounding areas. LULC mapping was conducted using Landsat and Sentinel images with supervised classification via a random forest classifier in Google Earth Engine. The area was categorized into nine LULC classes: built-up land, agricultural land, homestead vegetation, artificial water, grassland, forest, bare land, mudflat and seawater. The κ coefficients of the maps were high (> 0.71), indicating accurate classification. Built-up land was absent until 2014 and increased to 13.0 km^2 by 2021. Forest expanded from 32.6 km^2 in 1989 to 43.1 km^2 in 2014 but decreased to 36.0 km^2 by 2021. Transition matrix revealed that this decline was mainly due to the conversion of forest to built-up land (3.3 km^2), mudflat (2.3 km^2), bare land (2.2 km^2) and artificial water (2.1 km^2). Economic zone construction contributed to increases in built-up land, bare land and artificial water leading to forest loss and impacting the remaining forests. Moreover, substantial conversion of grassland into built-up and bare lands poses further threats to the ecological resilience of mangroves. Therefore, comprehensive monitoring, including the built-up surrounding areas, is crucial for timely and effective conservation efforts of mangrove forests.

Keywords Mangrove forest · Economic zone construction · Satellite images · Random forest· Land use and land cover (LULC) · Transition matrix

Introduction

Mangroves, a type of coastal wetlands, are woody plant communities thriving in the intertidal zones of tropical and subtropical coastlines and river mouths (Jia et al. 2023). They create a biodiverse and productive environment, offering numerous ecosystem services, including carbon sequestration for climate regulation, habitat and nursery grounds, coastal risk protection and cultural services such as ecotourism and education (Craft 2022). Mangroves have been recognized as a key component of national and international climate mitigation strategies in the land use, land-use change and forestry sector to support Nationally Determined Contributions under the Paris Agreement and advance the United Nations Sustainable Development Goals (Taillardat et al. 2018; Chow 2018).

Over the past century, 2/3 of mangroves have suffered irreversible damage (Long et al. 2023). Between 1990 and 2020, mangrove forest area declined by 1.04 million ha, with approximately 62% of the loss occurring between 2000 and 2016 (FAO 2020). These losses were mostly driven by forest clearing, wood extraction, population growth and urban expansion in coastal regions (Richards and Friess 2016; Thomas et al. 2017). In Bangladesh, mangroves have been impacted by tree felling and land conversion (Hasan et al. 2024), as well as urbanization, industrial exploitation, coastal development and agricultural reclamation, all of which directly affect land use and land cover (LULC) patterns (Kirwan and Megonigal 2013).

Special economic zones (SEZs) exemplify human-led activities that induce rapid LULC changes (Sosnovskikh 2017). Various countries have adopted SEZs to accelerate economic growth, attract foreign investment and promote industrialization (Tang 2022). However, few studies have assessed LULC changes resulting from SEZ establishment. Poorly planned LULC changes often lead to ecosystem degradation (Arshad et al. 2020), making spatiotemporal analysis around SEZ essential for monitoring human impacts (Ellis et al. 2011).

Bangladesh hosts the largest mangrove plantations in the world (Chowdhury et al. 2022), yet existing mangrove maps lack sufficient resolution to capture local-scale changes (Islam et al. 2019). While LULC changes in the central and western coastal zones have been well documented (Roy et al. 2024), the eastern zone remains underexplored, despite containing diverse mangrove plantations. This study focused on the Mirsharai-Sitakunda mangrove plantations in eastern Bangladesh. In response to the degradation of natural mangroves, the

Bangladesh government launched a coastal afforestation initiative in 1966 (Ullah et al. 2010), implemented by the Forest Department across various coastal regions (Barua and Rahman 2019). Coastal afforestation is considered a key strategy to enhance the resilience of country to climate change, given its high vulnerability to coastal hazards (Martin et al. 2020). Mangroves in this region play a crucial role in protecting against natural disasters but are undergoing LULC transformation due to human activities. The national SEZ adjacent to the Mirsharai and Sitakunda mangrove plantations is the focus of this study. Development activities, including infrastructure expansion, road construction, sand filling and tree felling, have affected nearby mangrove forests (Nabila and Tsuyuzaki 2025). Given the susceptibility to coastal disasters, such disturbances likely exacerbate environmental impacts. The proximity of the SEZ to mangrove forests suggests that LULC conversion due to construction reduces protection against flooding and high winds (Romañach et al. 2018). Quantitative estimates of LULC changes across spatial and temporal scales are therefore essential for understanding these impacts and informing policy interventions (Shawul and Chakma 2019). This study investigated the impact of SEZ development on mangrove forests by assessing spatiotemporal LULC changes over the past three decades.

Advances in satellite-based remote sensing (RS) have enabled timely and spatially explicit monitoring of LULC changes (Waleed et al. 2024). RS data are widely used due to their frequent observations and availability of free coarse-resolution imagery, which are processed in geographic information system (GIS) for accurate mapping (Tewabe and Fentahun 2020). RS applications have proven effective for mangrove inventory, mapping and change detection (Kirui et al. 2011). Google Earth Engine (GEE), a cloud-based platform for RS data, is commonly used in research for accessing multi-sensor imagery and metadata (Gorelick et al. 2017). GEE also provides pre-loaded machine learning models for applications, such as supervised LULC classification (Avci et al. 2023). The random forest (RF) algorithm is a widely used supervised classification method, offering advantages in feature selection and classification accuracy (Long et al. 2023).

Vegetation indices (VIs) derived from RS support reliable LULC classification in complex environments such as mangrove forests (Maryantika and Lin 2017). This study employed four VIs to improve classification accuracy: the Normalized Difference Vegetation Index (NDVI) and Soil-Adjusted Vegetation Index (SAVI) to distinguish mangrove from non-mangrove areas (Adamu et al. 2018); the Enhanced Vegetation Index (EVI) for mangrove classification (Akhtar and Tsuyuzaki 2024); and the modified Normalized Difference Water Index (mNDWI) to separate land and water features (Kelly and Gontz

2017). Elevation was also included as an auxiliary variable, as it interacts LULC distribution (Phan et al. 2020; Nasiri et al. 2022).

The objectives of this study were to: (a) extract and map LULC information before and after SEZ development; (b) detect changes over three decades; and (c) assess the transition dynamics of LULC classes due to construction activities. We argue that the current SEZ project underestimated its environmental impact on nearby mangrove forests and overlooked effects on more distant areas. These findings offer insights for policymakers regarding mangrove conservation and forest management in the context of development planning.

Materials and methods

Study area

The study area covers the Mirsharai-Sitakunda forests in the eastern coastal region of Bangladesh. In 1976, the Chittagong Coastal Afforestation Division initiated a mangrove afforestation program along the Mirsharai coastline (Fig. 1) to enhance coastal resilience (Uddin et al. 2014). The area was initially a bare mudflat, which remained unvegetated until successional processes facilitated the establishment of grasses (Saenger and Siddiqi 1993). In 2014, the Bangladesh Economic Zone Authority selected an area near the Mirsharai afforestation for economic zone development, based on its proximity to the Dhaka-Chittagong highway and the availability of land for industrial growth and infrastructure, including roads, drainage and power supply (BEZA 2014). Construction of buildings and roads was implemented as offsite facilities surrounding the economic zone. Since 2016, ongoing development activities within and around the zone have affected the nearby mangrove plantations. Therefore, the construction of the economic zone has disrupted these plantations, making this area a suitable site for study (22°34′-22°50′N and 91°23′-91°39′E, 5.3 m a.s.l.) (Fig. 1). The study area covered approximately 192 km^2, of which 122 to 144 km^2 were land, depending on coastal fluctuations.

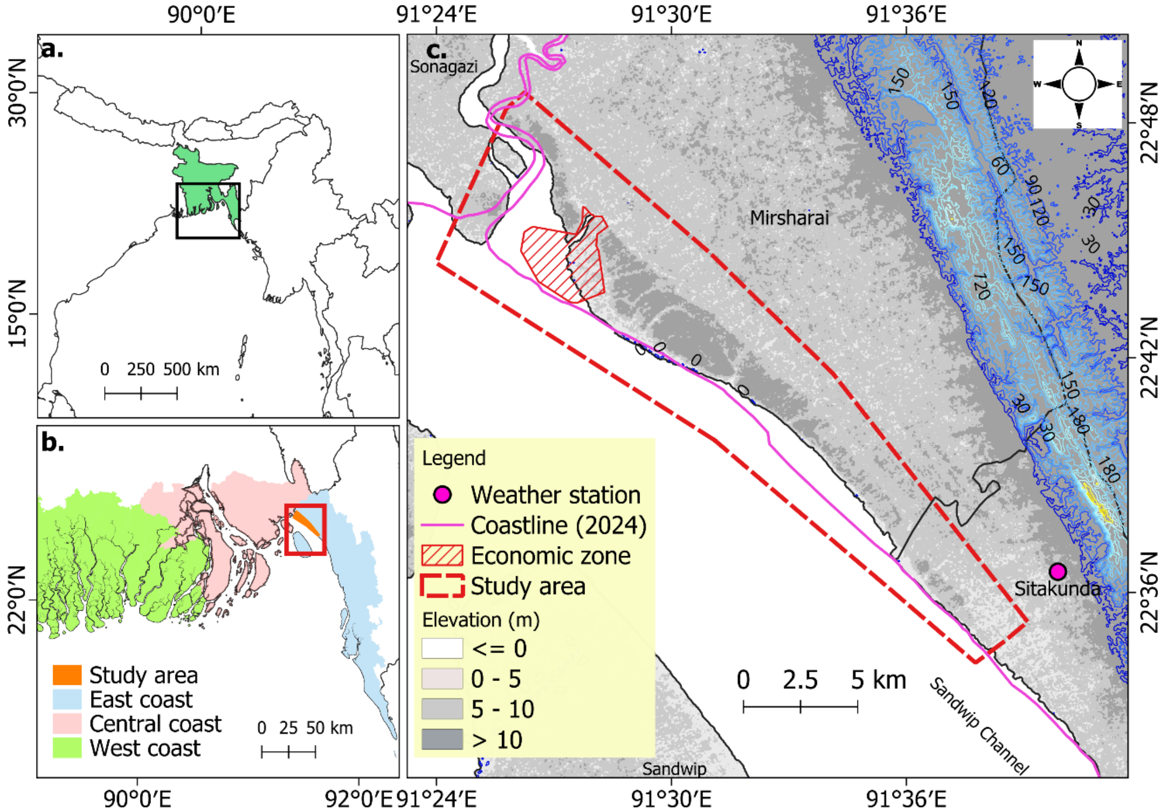

Fig. 1 Study site. (a) location of Bangladesh and neighboring countries; (b) study area along the eastern coast of Bangladesh; and (c) Mirsharai-Sitakunda coast showing with elevation, enclosed by dashed lines. Contour lines are shown at 30 m intervals. The economic zone was developed on the northern coast, which had extended over time through sedimentation

The climate in this region is categorized into tropical monsoon (Peel et al. 2007), with annual rainfall ranging from 2500 mm to 3000 mm (Brammer 2013). Maximum monthly temperatures reach 33.4°C, while minimums drop to 14.1°C. During the monsoon season, relative humidity averages 80% at a weather station approximately 4.5 km far from the study site. About 80% of the annual rainfall occurs between May to October (BMD 2023). Soil salinity ranges from 4 to 26 dS/m (SRDI 2010), and the slope direction of the terrain is oriented southwest toward the sea. Primary economic activities in this coastal region include farming, fishing and tourism (Ahmed et al. 2021).

Satellite image collection

This study used the satellite imagery from the GEE repository, which provides radiometrically and geometrically corrected datasets (Gorelick et al. 2017). RF classifier was employed in GEE due to its ability to handle multi-dimensional data, ignore irrelevant features, support flexible non-parametric modeling and accommodate missing data (Yuh et al. 2022). RF was selected to assess LULC changes in mangrove forests and surrounding areas. Five observation years were examined: 1989, 2001, 2011, 2014 and 2021. The 2014 image was used to capture land use types immediately prior to the construction of economic zone. Suitable cloud-free imagery was unavailable in 2015. The 2021 image was selected to detect post-construction human impact. A decadal interval was adopted to observe long-term changes, with the exception of 1990-1991, for which cloud-free imagery was unavailable during the target season; thus, a 1989 image was used instead (Purwanto et al. 2023).

Satellite images were accessed in GEE for: December 15 1989, February 7 2001, January 26 2011, February 19 2014 and January 26 2021. Sensors included Landsat 5 Thematic Mapper (TM), Landsat 7 Enhanced Thematic Mapper Plus (ETM+), Landsat 8 Operational Land Imager-Thermal Infrared Sensor (OLI-TIRS) and Sentinel 2A (Table 1). All images were acquired during winter under 0% cloud cover to minimize interannual variability (Bhattacharjee et al. 2021). LULC classification results indicated that interannual climate variability had limited influence on classification accuracy. Whenever available, Landsat Collection 2 Level-2 surface reflectance data, geometrically, radiometrically and atmospherically corrected by the United States Geological Survey (USGS), were used (Tesfaye et al. 2024). Landsat 5 was used in 2011 instead of Landsat 7 due to scan line errors. Sentinel 2A was selected for 2021 because no suitable cloud-free Landsat 8 imagery was available. Elevation data were sourced from the Shuttle Radar Topography Mission (SRTM) at 30 m resolution, provided by NASA and USGS/JPL-Caltech.

Table 1 Characteristics of satellite imagery used in this study

Sensor type	Platform	Acquisition date	Resolution (m)	Dataset Provider	Earth Engine Snippet
TM	Landsat 5	1989/12/15	30	USGS	ee.ImageCollection("LANDSAT/LT05/C02/T1_L2")
ETM+	Landsat 7	2001/02/07	30	USGS	ee.ImageCollection("LANDSAT/LE07/C02/T1_L2")
TM	Landsat 5	2011/01/26	30	USGS	ee.ImageCollection("LANDSAT/LT05/C02/T1_L2")
OLI-TIRS	Landsat 8	2014/02/19	30	USGS	ee.ImageCollection(“LANDSAT/LC08/C02/T1_L2”)
MultiSpectral Instrument	Sentinel-2A	2021/01/26	10	European Union/ ESA/Copernicus	ee.ImageCollection("COPERNICUS/S2")
SRTM	Endeavour (STS-99)	2000/ February	30	NASA/ USGS / JPL-Caltech	USGS/SRTMGL1_003

Image pre-processing

All collected images were processed using the GEE platform with its code editor (Kadri et al. 2023). To eliminate any haze, the cloud mask approach in GEE utilized the QA_PIXEL band for Landsat images and the QA60 band for Sentinel-2 image. The ee.FeatureCollection function was used to filter collections by specific date ranges. To enhance land cover categorization accuracy, auxiliary datasets were computed alongside spectral bands (Tesfaye et al. 2024). Four VIs were calculated for each image in GEE: NDVI (Tucker 1979), EVI (Huete et al. 2002), SAVI (Huete 1988) and mNDWI (Xu 2006) using the following equations:

$$NDVI = (NIR - red)/(NIR + red) \quad (1)$$

$$SAVI = \{(NIR - red)/(NIR + red + L)\} \times (1 + L) \quad (2)$$

$$EVI = G \times \{(NIR - red)/(NIR + C1 \times red - C2 \times blue + L)\} \quad (3)$$

$$mNDWI = (green - SWIR)/(green + SWIR) \quad (4),$$

where reflectance in specific spectrum components is denoted as blue, green, red, near-infrared (NIR) and shortwave infrared (SWIR). G denotes a gain factor (Eq. 3), L is a soil adjustment factor (Eqs. 2 and 3) and C_1 and C_2 are coefficients used to correct aerosol scattering in the red band using the blue band (Jiang et al. 2008). For EVI, the following parameters were used: G = 2.5, C_1 = 6 and C_2 = 7.5 and L = 1. For SAVI, L = 0.5 was applied. SRTM digital elevation data were incorporated to improve dataset accuracy (Farr et al. 2007).

LULC classes

Based on field observations conducted in November 2021, the study area was classified into nine land cover classes: built-up land, agricultural land, homestead vegetation, artificial water, grassland, forest, bare land, mudflat and seawater (Table 2).

Table 2 Description of LULC classes used in this study

LULC	Description
Built-up land	Industrial area, roads, dyke and other establishments associated with the economic zone
Agricultural land	Land used for crop production and grazing, fallow land (Fig. S1)
Homestead vegetation	Vegetation planted around rural settlements/homesteads, roadside vegetation
Artificial water	Aquaculture ponds, lakes, waterlogged area associated with the economic zone establishment
Grassland	Area covered with grass, dominated by *Porteresia coarctata* (Roxb.) Tateoka (Poaceae), a pioneer on coastlines in the northern Bay of Bengal (Naskar et al. 2021)
Forest	Planted mangrove forest
Bare land	Barren land, exposed soil
Mudflat	Coastal flat, marsh and newly accreted land
Seawater	Open sea, channel, creeks

Training and validation samples for LULC classification

A common technique for obtaining training and validation samples involves the visual interpretation of high-resolution satellite imagery (Li et al. 2019). In this study, LULC classification was performed using training samples derived from high-resolution Google Earth imagery. Ground truth data were collected from accessible areas using a handheld GPS device (GPSmap 60CSx, Garmin, Schaffhausen, Switzerland) to validate land cover classes through field inspection. Historical maps and records from the Bangladesh Forest Department were consulted; however, visual interpretation was primarily employed to validate classifications of earlier imagery. The number of collected samples, stratified by land cover class, ranged from 1853 to 2832 pixels. Sample size per class was determined by the distribution and abundance of each land cover class (Ghosh et al. 2016). Of the total samples, 70% were allocated for training and 30% for validation (Loulad et al. 2023).

Supervised classification was conducted using the RF machine learning algorithm, which is widely recognized for its high classification accuracy (Ramezan et al. 2021). The performance of RF algorithm depends on the number of trees and selected parameters (Patil and Panhalkar 2023). In this study, RF parameters were set to 300 trees and five features per node split (Kouassi et al. 2023).

Accuracy assessment and post-processing

After classification, a confusion matrix was used to evaluate each classified image (Midekisa et al. 2017). Classification performance and errors were assessed using overall accuracy (OA), κ coefficient, user accuracy (UA) and producer accuracy (PA). OA represents the percentage of correctly classified test samples (Tesfaye et al. 2024). The κ, ranging from 0 to 1, measures agreement beyond chance, with values between 0.61 and 0.80 considered substantial (McHugh 2012). PA was calculated by dividing the number of correctly classified reference samples by the total number of reference samples for that class. UA was calculated by dividing the number of correct classifications for a given class by the total number of predicted samples for that class (Aji et al. 2023). To minimize classification error, the procedure was repeated multiple times using different datasets. Both quantitative and qualitative metrics, including visual inspection, were used to evaluate the results. Field investigations and prior knowledge were incorporated to verify outcomes. To validate the LULC classification, a cross-validation was performed by 205 ground truth points, with 15 to 35 samples per class. Final LULC maps for each year underwent post-processing using classification sieve corrections in QGIS (version 3.16.15), which replaces isolated pixels with those of the largest neighboring patch (Congedo 2021).

LULC change assessment

The area covered by classified LULC maps for each specified period was calculated and temporal variations were quantified. Post-classification comparison techniques based on ‘from-to’ change information were applied to identify LULC changes over time (Ghosh et al. 2016). Absolute changes in LULC categories were calculated as the difference between two successive LULC maps (Shawul and Chakma 2019). Transition matrices were constructed to illustrate the conversion patterns among LULC category.

Results

LULC classification accuracy

Table 3 Accuracy assessment of LULC classification. PA = Producer accuracy (%); UA = User accuracy (%)

Year	1989		2001		2011		2014		2021		Average PA	Average UA
LULC	PA	UA	PA	UA	PA	UA	PA	UA	PA	UA		
Built-up land	-	-	-	-	-	-	-	-	96	97	96	97
Agricultural land	77	75	79	76	72	88	83	86	73	71	76.8	79.2
Homestead vegetation	73	67	65	79	73	61	78	74	73	63	72.4	68.8
Artificial water	82	75	54	56	74	65	96	81	93	84	79.8	72.2
Grassland	88	85	67	61	72	66	69	85	69	57	73.0	70.8
Forest	76	83	83	74	84	90	88	87	88	92	83.8	85.2
Bare land	88	80	89	94	67	64	67	67	56	70	73.4	75.0
Mudflat	93	93	90	84	71	85	84	92	68	80	81.2	86.8
Seawater	95	97	87	87	90	80	97	88	85	87	90.8	87.8
Overall accuracy (%)	80		79		79		84		81			
κ-coefficient	0.75		0.73		0.71		0.79		0.77			

κ exceeded 0.71 in all five assessments (Table 3), with OA above 79%, showing the reliability of LULC classification. PAs were over 90% for seawater in 1989, 2011 and 2014, mudflat in 1989 and 2001, and artificial water in 2014 and 2021 and built-up land in 2021. All PAs exceeded 65%, except for artificial water in 2001 (54%) and bare land in 2021 (56%). UA in 1989 ranged from 67% for homestead vegetation to 97% for seawater. In 2001, UA varied from 56% for artificial water to 94% for bare land. In 2011, UA ranged from 61% for homestead vegetation to 90% for forest. UA in 2014 ranged from 67% for bare land to 92% for mudflat. In 2021, built-up land showed the highest UA at 97%. Overall, built-up land, agricultural land, forest, mudflat and seawater showed relatively high UA.

Landsat images in 1989 (80%, κ = 0.75), 2001 (79%, 0.73), 2011 (79%, 0.71) and 2014 (84%, 0.79) yielded comparable OA and κ to those derived from the Sentinel 2A image in

2021 (81%, 0.77). However, the confusion matrix revealed misclassification between forest and homestead vegetation (Table 4). Additional confusion was observed between grassland and homestead vegetation and occasionally between artificial water and seawater (Table S1).

Table 4 Confusion matrix showing misclassification among LULC types and classification accuracies for 1989

LULC	Agricultural land	Homestead vegetation	Artificial water	Grassland	Forest	Bare land	Mudflat	Seawater	Total	User Accuracy (%)
Agricultural land	27	2	0	5	0	2	0	0	36	75
Homestead vegetation	2	157	0	2	74	1	0	0	236	67
Artificial water	0	0	9	2	0	0	0	1	12	75
Grassland	1	3	0	107	7	2	5	1	126	85
Forest	0	53	0	0	253	0	0	0	306	83
Bare land	5	1	0	3	0	37	0	0	46	80
Mudflat	0	0	1	3	0	0	85	2	91	93
Seawater	0	0	1	0	1	0	1	84	87	97
Total	35	216	11	122	335	42	91	88	940	
Producer Accuracy (%)	77	73	82	88	76	88	93	95		

Spatiotemporal changes in LULC

The LULC map showed that, except for seawater, the majority of the area was covered with forest (Fig. 2), stretching between seawater and agricultural land. Homestead vegetation was primarily located on the eastern side, adjacent to agricultural land, throughout the studied period from 1989 to 2021. Artificial water was distributed mostly in the northern region, near built-up land. Over time, the coastline expanded mainly in the northern part of the study area (Fig. 2). This region exhibited considerable variability, driven mostly by natural processes. However, the establishment of the SEZ appears to have constrained these natural fluctuations.

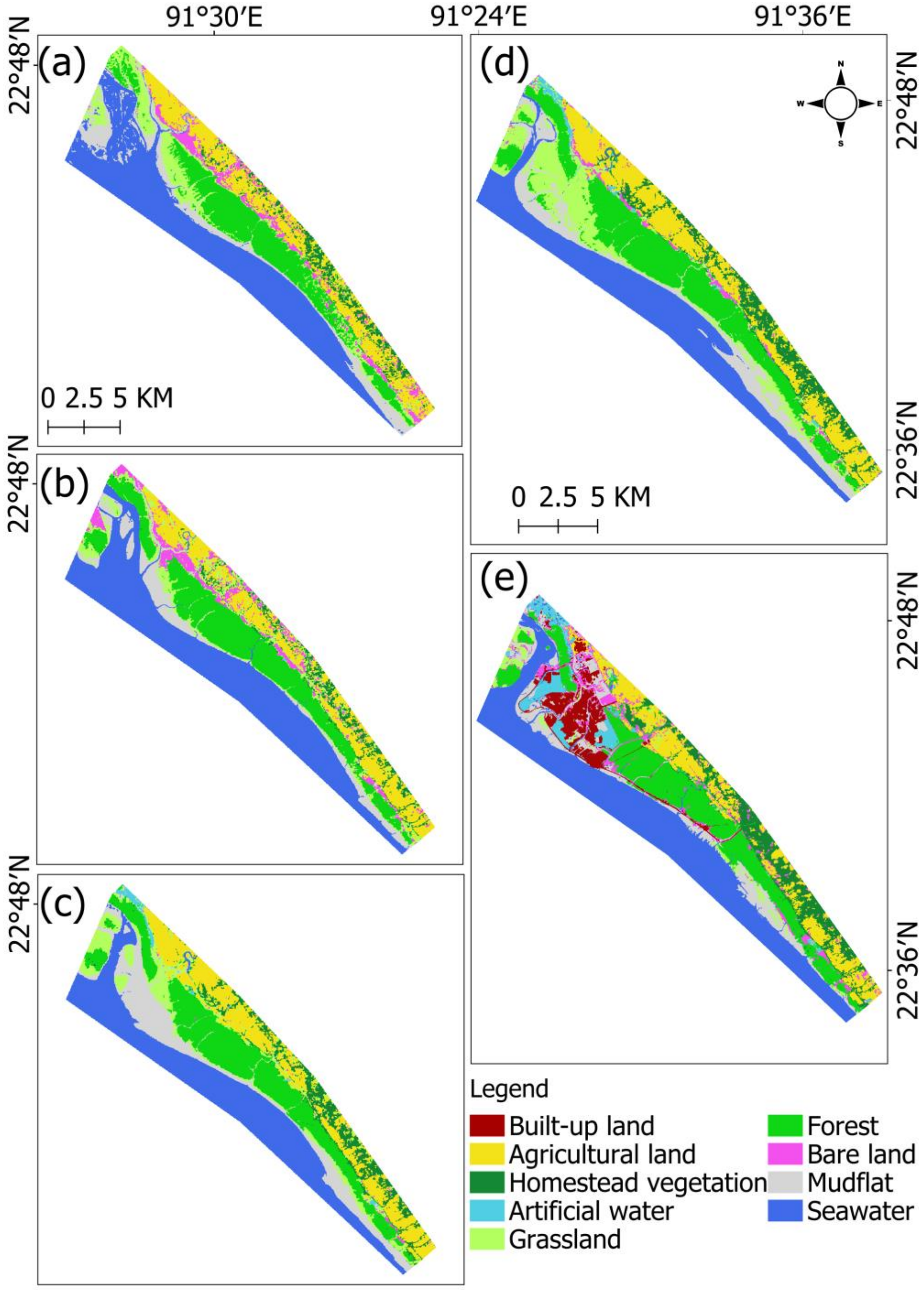

Fig. 2 The LULC maps showing the distribution of examined LULC classes in (a)1989; (b) 2001; (c) 2011; (d) 2014; and (e) 2021

In 2014, there was no built-up area, indicating minimal human disturbances (Fig. 3). Built-up land was not observed until 2014 and appeared in 2021 mostly in the northwestern parts and extended into the middle of the forest. In addition, along approximately half of the coastline, mangroves were severed from direct seawater connectivity, thereby compromising their coastal protection functions (Fig. 4B).

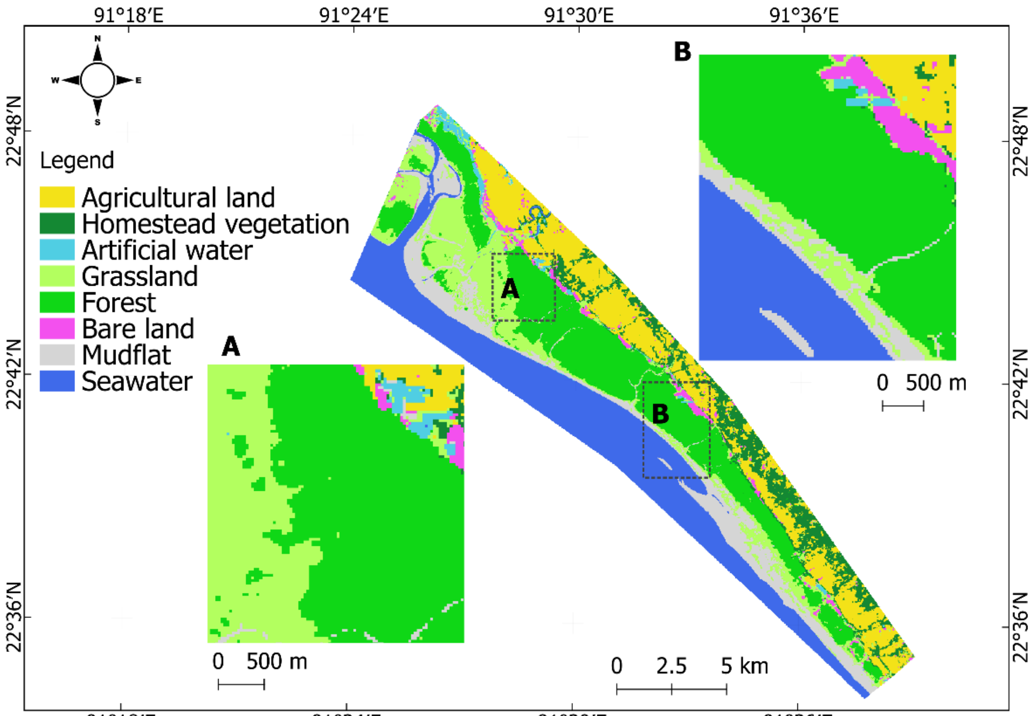

Fig. 3 Distribution of LULC types in 2014 (Panels A and B show zoom-in views of two selected areas at different spatial scales)

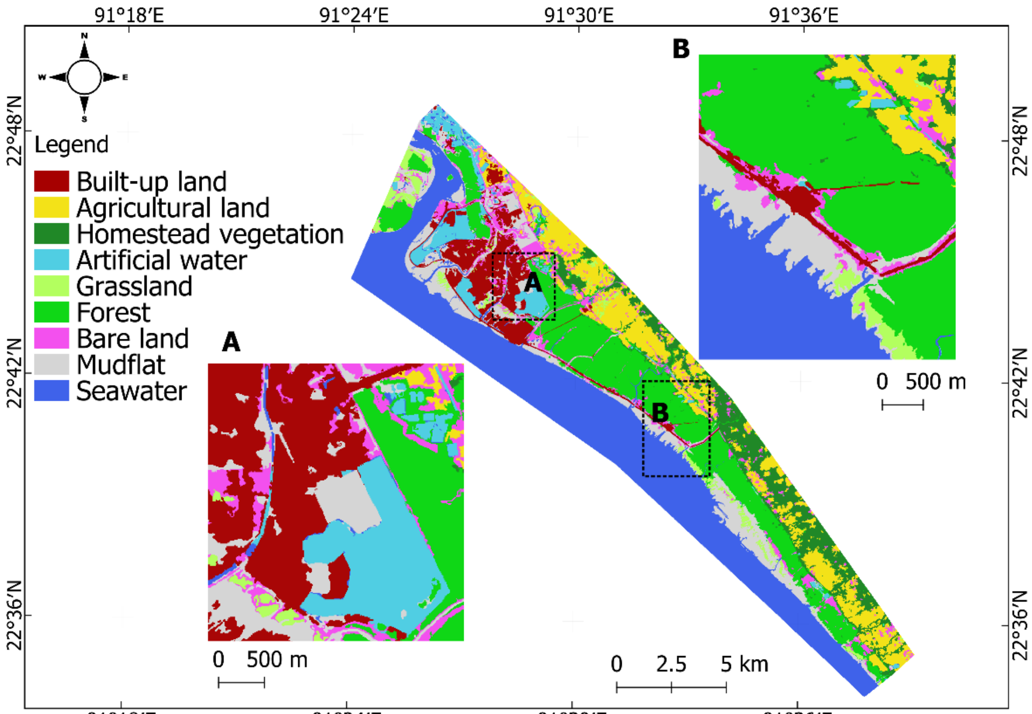

Fig. 4 LULC map magnified to examine the effects of built-up land in 2021 (Panels A and B show zoom-in views of two selected areas at different spatial scales)

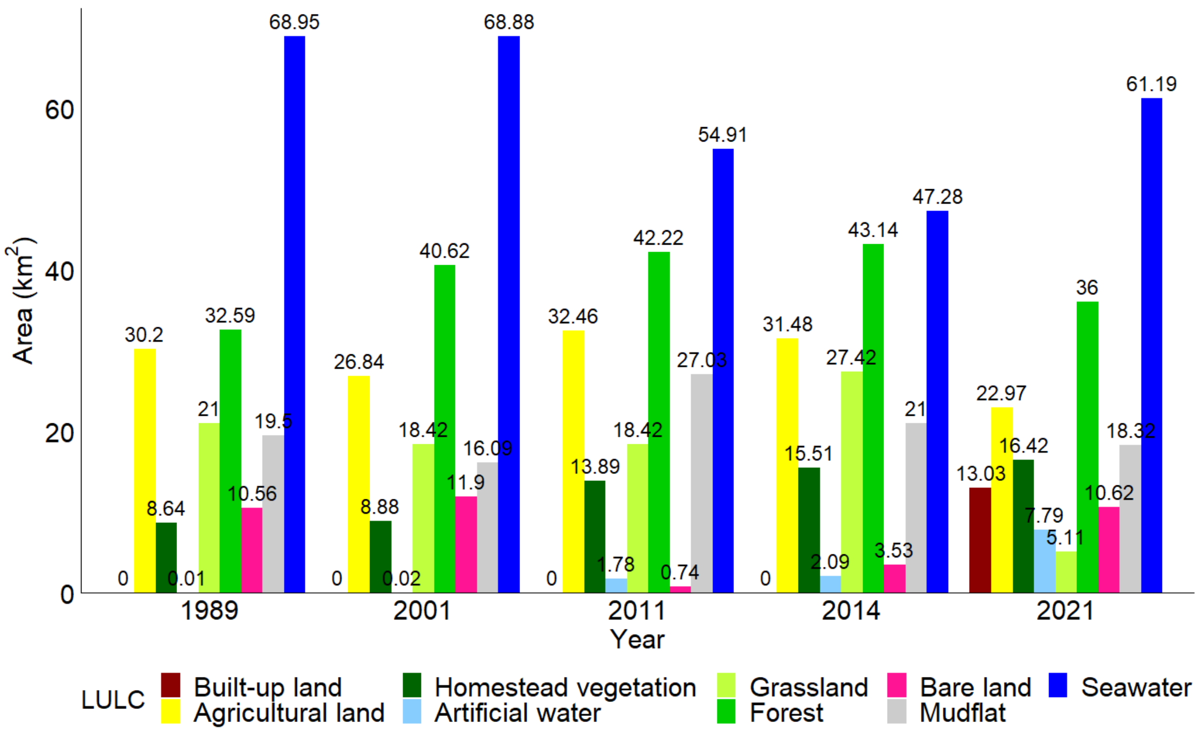

Fig. 5 Temporal changes in LULC areas from 1989 to 2021, illustrating land cover transitions over the study period

Built-up land was absent until 2014 but expanded to 13.0 km^2 in 2021 (Fig. 5). Agricultural land decreased from 30.2 km^2 in 1989 to 22.9 km^2 in 2021. Homestead vegetation increased steadily, from 8.7 km^2 in 1989 to 16.4 km^2 in 2021. Artificial water bodies expanded from less than 0.1 km^2 in 1989 to 7.8 km^2 in 2021. Grassland decreased substantially, from 21.0 km^2 in 1989 to 5.1 km^2 in 2021. Forest cover increased from 32.6 km^2 in 1989 to 40.6 km^2 in 2001, 42.2 km^2 in 2011 and 43.1 km^2 in 2014, but then declined to 36.0 km^2 in 2021. Bare land decreased from 10.6 km^2 in 1989 to 3.5 km^2 by 2014, then returned to 10.6 km^2 in 2021. Mudflat area fluctuated over time: it decreased from 19.5 km^2 in 1989 to 16.1 km^2 by 2001, increased to 27.1 km^2 in 2011 and dropped again to 18.3 km^2 in 2021. Seawater was 68.9 km^2 in 1989 and decreased to 61.2 km^2 in 2021.

From 1989 to 2021, seawater, mudflat, grassland and agricultural land decreased, while artificial water bodies, homestead vegetation and built-up land increased (Table 5). However, the magnitude and direction of changes varied across sub-periods: 1989 to 2001, 2001 to 2011, 2011 to 2014 and 2014 to 2021. Forest area declined between 2014 and 2021, despite earlier gains, primarily due to conversion into built-up land and mudflat. Grassland also declined after 2014, primarily transitioning into mudflat and built-up land.

Table 5 Changes in LULC areas (km^2) from 1989 to 2021. Red shading indicates a decrease and green shading indicates an increase. The intensity of each color, ranging from light to dark, reflects the magnitude of change

	LULC change					
Class	1989-2001	2001-2011	2011-2014	2014-2021	Net (1989-2021)	
					Km^2	%
Built-up land	0.00	0.00	0.00	13.03	13.03	6.80
Agricultural land	-3.36	5.62	-0.98	-8.51	-7.23	-3.78
Homestead vegetation	0.24	5.01	1.62	0.91	7.78	4.07
Artificial water	0.01	1.75	0.32	5.70	7.78	4.06
Grassland	-2.77	0.19	9.00	-22.31	-15.89	-8.29
Forest	8.03	1.60	0.92	-7.14	3.41	1.77
Bare land	1.34	-11.16	2.79	7.09	0.06	0.05
Mudflat	-3.41	10.94	-6.03	-2.68	-1.18	-0.62
Seawater	-0.07	-13.97	-7.63	13.91	-7.76	-4.06

Between 1989 and 2001, 54% of the area (102.7 km^2) remained unchanged in terms of LULC, including 15% of forest (28.9 km^2) that persisted without alteration (Fig. 6). Non-forest changes accounted for 44.4 km^2 (23%) of the total area. During this period, forest increased by 11.7 km^2 (6%), mostly in the north region, while it decreased by 3.7 km^2 (2%) in the central part of the study area.

Between 2001 and 2011, 99.3 km^2 (55%) of the area remained unchanged, including 38.2 km^2 of stable forest (20%). During this period, forest increased by 4.0 km^2 (2%) and decreased 2.4 km^2 (1%), resulting in a net gain. From 2011 to 2014, 106.5 km^2 (56%) showed no change, with 39.7 km^2 (21%) classified as forest. Forest expansion continued (3.4 km^2, 2%), although 2.5 km^2 (1%) was lost prior to development activities. Meanwhile, 38.1 km^2 (21%) underwent non-forest transitions. From 2014 to 2021, forest loss totaled 11.2 km^2 (6%), occurring both in the northern sector and within interior forest areas distant from the project zone. New road networks emerged across the landscape, including areas outside the economic zone. Non-forest changes accounted for 55.7 km^2 (29%), while 88.7 km^2 (46%) remained stable, including 31.9 km^2 (17%) of persistent forest. Despite ongoing degradation, forest increased by 4 km^2 (2%) during this period.

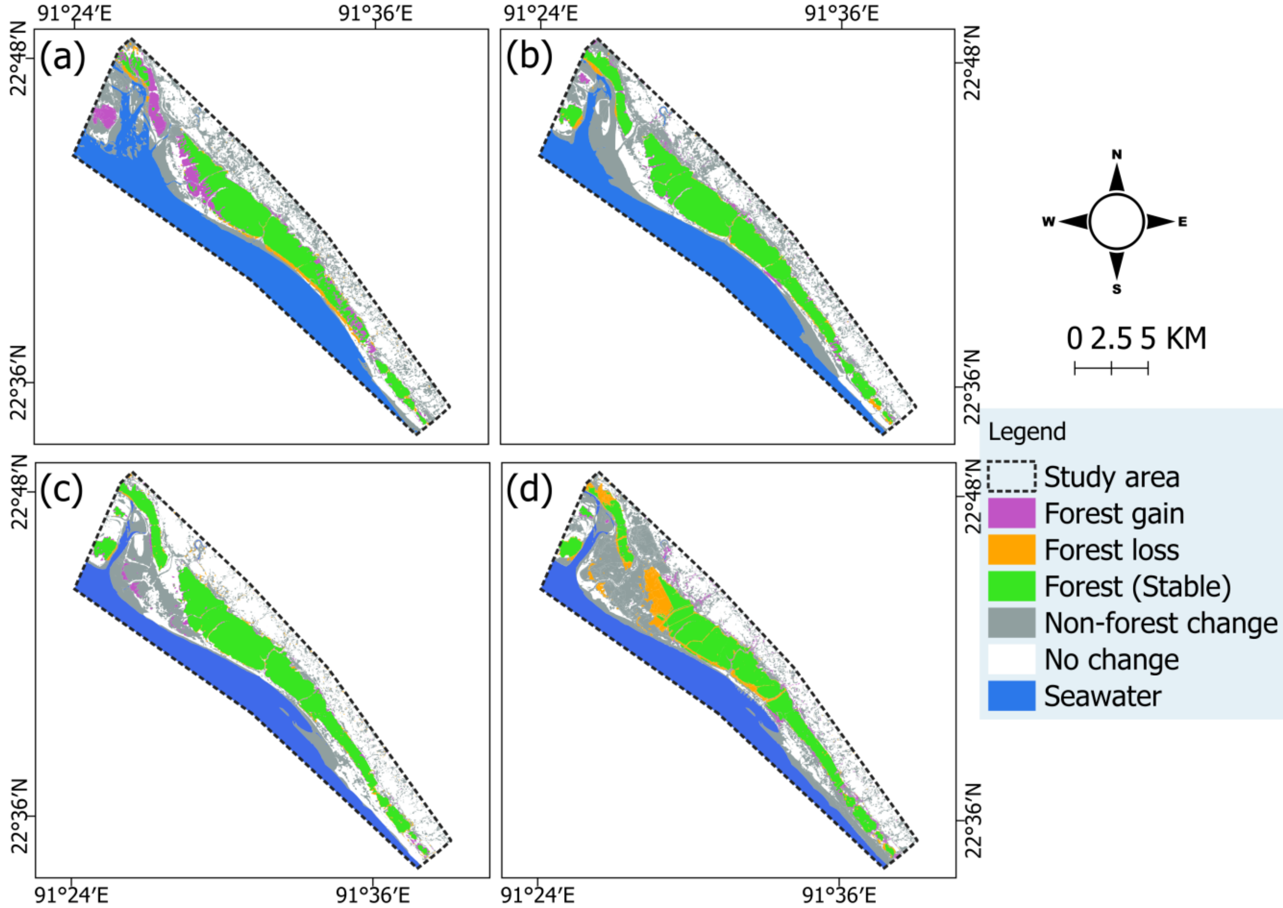

Fig. 6 Change in LULC over time: (a) from 1989 to 2001; (b) from 2001 to 2011; (c) from 2011 to 2014; and (d) from 2014 to 2021

LULC transformation from 1989 to 2021

Between 1989 and 2001, 28.9 km^2 of the total 32.6 km^2 forest area were unchanged, while minor conversions occurred to grassland (1.5 km^2), mudflat (0.8 km^2) and seawater (0.9 km^2) (Table 6). Of the 30 km^2 of agricultural land in 1989, 21.4 km^2 persisted through 2001, with 3.8 km^2 transitioning to grassland and 3.3 km^2 to bare land. Conversely, bare land contributed 2.8 km^2 to agricultural land and 2.2 km^2 to grassland. Grassland underwent notable conversions to forest (9.7 km^2) and bare land (3.3 km^2).

Table 6 Transition matrix of LULC changes (km^2) between 1989 and 2001

Year	LULC	2001: Built-up land	Agricultural land	Homestead vegetation	Artificial water	Grassland	Forest	Bare land	Mudflat	Seawater
1989	Built-up land	**0.00**	0.00	0.00	0.00	0.00	0.00	0.00	0.00	0.00
	Agricultural land	0.00	**21.43**	1.57	0.00	3.79	0.04	3.31	0.04	0.02
	Homestead vegetation	0.00	1.82	**5.09**	0.00	1.49	0.09	0.14	0.00	0.00
	Artificial water	0.00	0.00	0.00	**0.00**	0.01	0.00	0.00	0.00	0.00
	Grassland	0.00	0.68	1.20	0.00	**4.59**	9.74	3.32	0.92	0.56
	Forest	0.00	0.02	0.30	0.00	1.47	**28.93**	0.13	0.81	0.92
	Bare land	0.00	2.83	0.65	0.00	2.22	0.43	**4.21**	0.13	0.08
	Mudflat	0.00	0.03	0.05	0.01	3.42	1.19	0.75	**7.07**	6.97
	Seawater	0.00	0.01	0.01	0.00	1.24	0.20	0.03	7.12	**60.33**

Bold numbers represent unchanged LULC areas between 1989 and 2001 (km^2)

From 2001 to 2011, mudflat was replaced mostly by grassland (4.3 km^2), while seawater remained largely stable at 52.7 km^2. Coastal expansion was evident, with 15.3 km^2 of seawater converting to mudflat, increasing its total area from 16.1 km^2 to 27.1 km^2 (Table 7). Bare land changed to agricultural land (5.7 km^2) and grassland (4.0 km^2). Forests showed modest expansion during this period.

Table 7 Transition matrix of LULC changes (km^2) between 2001 and 2011

Year	LULC	2011: Built-up land	Agricultural land	Homestead vegetation	Artificial water	Grassland	Forest	Bare land	Mudflat	Seawater
2001	Built-up land	**0.00**	0.00	0.00	0.00	0.00	0.00	0.00	0.00	0.00
	Agricultural land	0.00	**22.76**	2.63	0.04	1.16	0.08	0.15	0.00	0.02
	Homestead vegetation	0.00	0.70	**7.06**	0.01	0.33	0.74	0.00	0.02	0.00
	Artificial water	0.01	0.00	0.00	**0.00**	0.00	0.00	0.00	0.00	0.01
	Grassland	0.00	3.26	3.44	0.60	**6.77**	2.41	0.43	1.17	0.43
	Forest	0.00	0.01	0.39	0.02	0.99	**38.20**	0.05	0.64	0.32
	Bare land	0.00	5.72	0.34	0.86	4.02	0.32	**0.37**	0.26	0.00
	Mudflat	0.00	0.02	0.03	0.22	4.33	0.40	0.02	**9.64**	1.43
	Seawater	0.00	0.00	0.00	0.01	0.81	0.08	0.00	15.31	**52.67**

Bold numbers represent unchanged LULC areas between 2001 and 2011 (km^2)

Table 8 Transition matrix of LULC changes (km^2) between 2011 and 2014

Year		2014								
	LULC	Built-up land	Agricultural land	Homestead vegetation	Artificial water	Grassland	Forest	Bare land	Mudflat	Seawater
2011	Built-up land	**0.00**	0.00	0.00	0.00	0.00	0.00	0.00	0.00	0.00
	Agricultural land	0.00	**27.82**	2.40	0.09	0.55	0.05	1.52	0.03	0.01
	Homestead vegetation	0.00	1.84	**10.91**	0.03	0.35	0.69	0.06	0.00	0.01
	Artificial water	0.00	0.03	0.05	**1.18**	0.29	0.07	0.07	0.05	0.02
	Grassland	0.00	1.43	1.37	0.40	**11.31**	1.41	1.49	0.77	0.24
	Forest	0.00	0.09	0.57	0.18	1.06	**39.74**	0.13	0.25	0.20
	Bare land	0.00	0.21	0.08	0.02	0.19	0.07	**0.16**	0.00	0.00
	Mudflat	0.00	0.01	0.04	0.16	12.96	0.96	0.09	**11.16**	1.65
	Seawater	0.00	0.03	0.08	0.03	0.72	0.14	0.00	8.73	**45.16**

Bold numbers represent unchanged LULC areas between 2011 and 2014 (km^2)

Between 2011 and 2014, 12.9 km^2 of mudflat areas were converted to grassland, contributing to the expansion of grassland (Table 8). Agricultural land underwent transitions, with 2.4 km^2 converted to homestead vegetation and 1.5 km^2 to bare land, while 27.8 km^2 remained unchanged in 2014. Prior to development, the mangrove forest exhibited a net increase in area during the period.

Table 9 Transition matrix of LULC changes (km^2) between 2014 and 2021

Year		2021								
	LULC	Built-up land	Agricultural land	Homestead vegetation	Artificial water	Grassland	Forest	Bare land	Mudflat	Seawater
2014	Built-up land	**0.00**	0.00	0.00	0.00	0.00	0.00	0.00	0.00	0.00
	Agricultural land	1.43	**19.31**	3.93	0.40	0.88	0.43	3.56	1.46	0.08
	Homestead vegetation	0.02	1.86	**11.43**	0.09	0.05	1.20	0.72	0.12	0.04
	Artificial water	0.05	0.04	0.03	**1.27**	0.01	0.21	0.11	0.13	0.24
	Grassland	7.22	0.40	0.47	2.75	**2.79**	1.59	2.79	6.88	2.54
	Forest	3.25	0.10	0.44	2.06	0.27	**31.99**	2.21	2.29	0.54
	Bare land	0.22	1.21	0.12	0.19	0.10	0.23	**0.95**	0.44	0.06
	Mudflat	0.85	0.01	0.01	1.03	0.98	0.35	0.21	**6.39**	11.17
	Seawater	0.01	0.04	0.00	0.01	0.02	0.01	0.07	0.61	**46.52**

Bold numbers represent unchanged LULC areas between 2014 and 2021 (km^2)

Between 2014 and 2021, built-up land emerged, resulting in a reduction of agricultural land by 1.4 km^2 and increase in bare land by 3.6 km^2. Forests declined following the construction of SEZ after 2016, with 3.3 km^2 converted to built-up land and 2.3 km^2 to mudflat. In addition, 2.2 km^2 of forest was converted to bare land and 2.1 km^2 to artificial water. Grassland was converted to built-up land (7.2 km^2) and mudflat (6.9 km^2). Mudflat areas decreased by 11.2 km^2, mostly converted to seawater (Table 9).

Discussion

The accuracy of the LULC classification remained relatively consistent across the study periods. By incorporating auxiliary data, satisfactory performance was achieved, with OA exceeding 79% and κ greater than 0.71. Nonetheless, persistent misclassifications were observed between forests and other vegetated classes, due to their similar spectral signatures (Otero et al. 2016). Annual fluctuations in classification accuracy for categories such as artificial water and bare land appear to be associated with the dispersed and infrequent spatial distribution of these classes (Abdullah et al. 2019). Spectral similarities among homestead vegetation, grassland and forest further contribute to classification errors, resulting in reduced accuracy for these categories. In addition, LULC classification in heterogenous coastal areas tends to favor majority classes, potentially leading to misclassification of minority classes (He and Garcia 2009).

LULC maps from 1989 to 2021 illustrated the spatial distribution of LULC classes across five distinct time periods. The temporal analysis revealed substantial transformations in landscape composition over the study periods. Particularly, two distinct change patterns were identified for the mangrove forest. In the central region, mangroves formed a natural barrier between coastal and inland zones. From 1989 to 2014, the forest area exhibited an increasing trend, primarily driven by afforestation initiatives under various coastal restoration projects (Hoque et al. 2021). This expansion was supported by both natural regeneration and targeted afforestation efforts (Uddin et al. 2014). However, a marked decline in mangroves was observed between 2014 and 2021, mostly due to built-up development associated with the economic zone (Uddin et al. 2022). Built-up land exhibited monotonic increase throughout the study period, with expansion concentrated near the project zone and adjacent development areas. These changes reflect the spatial influence of infrastructure growth and land conversion pressures in coastal regions.

Furthermore, the findings revealed declining trends in seawater, mudflat, grassland and agricultural land, while artificial water bodies, homestead vegetation, bare land and built-up land exhibited increasing trends. The expansion of homestead vegetation occurred primarily at the expense of agricultural land (Islam et al. 2022) along the eastern margin of the study area, driven by population growth (Hoque et al. 2020). Although homestead vegetation represents a multifunctional vegetation system designed to support livelihoods, subsistence needs and environmental conservation, its expansion has led to loss in ecosystem services, including crop production, soil formation and water infiltration. Government-led initiatives, such as the promotion of fruit trees, fuelwood species and forest plantations around rural homesteads, along with the coastal green belt project for mangrove restoration, have contributed to the protection of ecosystem services despite the reduction of agricultural land (Hoque et al. 2022). However, as population pressures continue to rise, the risk of overexploitation should be considered in conservation planning (Rahman et al. 2018). Agricultural land was also converted into built-up and bare land, likely driven by infrastructural expansion and land development activities.

Since 2016, mangrove forests have been increasingly replaced by construction activities, such as road construction, sand filling, tree felling and dyke construction. These interventions have led to the conversion of mangrove forests into built-up land, mudflat, bare land, and artificial water bodies. The development of economic zones has been a major driver of forest loss (Aung et al. 2022), particularly in the northern regions where built-up expansion was most pronounced (Nabila and Tsuyuzaki 2025). Infrastructure projects, such as roads, sluice gates and dykes, have facilitated greater access to forest resources, thereby accelerating degradation (Daigle 2010; Benfield et al. 2005). Mangroves often experience water deficits due to restricted hydrological flow caused by artificial barriers and adjacent built-up zones (Arshad et al. 2020). Roads constructed within mangroves contribute to ecological fragmentation by impeding the exchange of water, nutrients and biota (Din et al. 2017). Such developments promote unsustainable resource exploitation, environmental deterioration and biodiversity loss (Agbagwa and Ndukwu 2014). Moreover, paved roads often lead to the proliferation of unpaved road networks, enhancing access to mangrove areas (Hayashi et al. 2019). Post-construction landscapes are occasionally colonized by non-forest plants, altering native vegetation dynamics (Van Vliet 2019). Excavation of artificial water bodies, such as lakes and ponds, for economic zone development has also contributed to the conversion of mangroves and grasslands. The replacement of grasslands with built-up areas is concerning, as grass plays a critical role in enhancing coastal resistance and stabilizing sediment

(McConchie and Saenger 1991). Mangrove degradation has profound implications for coastal ecological stability (Suratman 2008). The conversion of natural habitats into human-induced land uses poses a threat to the survival of local ecosystems (Islam et al. 2016). The impacts of construction activities extend beyond immediate project sites, affecting distant forest and coastal areas through hydrological and ecological connectivity.

The impact of built-up land and associated development activities on forest ecosystems should be carefully considered when evaluating the sustainability of adjacent forested areas. Forest conversion to built-up land or other land use classes increases ecological vulnerability and disrupts landscape integrity (Fan et al. 2024). Such transformations often require the removal of natural vegetation, including forests and grasslands, leading to the loss of green spaces and fragmentation of ecological networks (Miah et al. 2024). Mangrove degradation resulting from intensive LULC changes should foster a false sense of security among local communities by offering less coastal protection than perceived (Chow 2018). Although an environmental impact assessment was conducted prior to economic zone development, its scope underestimated the broader ecological consequences. Our findings demonstrate that the impacts of economic zone construction extend beyond immediate forest boundaries and affect distant areas. Given the accelerating pace of human activity and climate change, LULC patterns are expected to shift rapidly, with implications for regional ecosystems and community livelihoods (Islam et al. 2022). Human disturbances will likely intensify mangrove vulnerability and compromise climate adaptation capacity. However, improved management of such disruptions can enhance the resilience and resistance of mangrove ecosystems to sea level rise and other climate-related stresses (Gilman et al. 2008). To safeguard remaining mangrove forests and mitigate adverse impacts, comprehensive and enhanced environmental impact assessments should be conducted prior to initiating development projects near coastal ecosystems. Integrated conservation strategies are essential and should include replanting mangrove trees on suitable accreted land, preventing illegal encroachment, monitoring artificial expansion of water bodies and enacting effective mangrove protection policies.

Conclusion

LULC changes were mapped and quantitatively assessed from 1989 to 2021 in the eastern coastal mangrove areas of Bangladesh. Forest cover increased from 1989 to 2014; however, the subsequent period witnessed a decline, accompanied by the emergence of built-up land and the expansion of artificial water bodies, particularly between 2014 and 2021. The transition matrix revealed substantial LULC transformations during this period, largely driven by the establishment of the economic zone project, indicating that human activities altered the existing landscape. The conversion of forests to built-up land and bare land, both near and distant from the economic zone, suggests that intensive construction activities have disrupted the integrity of the coastal mangrove ecosystems. In addition, the transformation of grasslands into built-up and bare land poses further threats to the ecological resilience and stability of mangrove ecosystems. This study employed transition matrices to generate spatial data on LULC changes and highlighted the extent of transformation due to human impact. The resulting spatial database offers valuable insights for forest management and conservation planning. It supports policymakers and planners in balancing development with ecological protection and emphasizes the importance of incorporating the broader impacts of development projects into forest management strategies for coastal regions.

Declarations

Conflict of interest

The authors declare that they have no conflict of interest.

Ethics approval

No ethical approval was required.

Funding

This work is partly supported by JSPS (Japan Society for the Promotion of Science), MEXT (Ministry of Education, Culture, Sports, Science and Technology), and RESTEC (Remote Sensing Technology Center of Japan).

Authors' contribution statements

Conceptualization: Irtifa Alam Nabila, Shiro Tsuyuzaki; Methodology: Irtifa Alam Nabila; Formal analysis and investigation: Irtifa Alam Nabila; Writing - original draft preparation: Irtifa Alam Nabila; Writing - review and editing: Irtifa Alam Nabila, Shiro Tsuyuzaki;

Funding acquisition: Shiro Tsuyuzaki; Resources: Shiro Tsuyuzaki; Supervision: Shiro Tsuyuzaki

Acknowledgements

We are grateful to the United States Geological Survey and the European Space Agency for providing Landsat and Sentinel-2A data freely accessible. We also thank Md. Mamsed Hasan, Md. Nurul Azam and others for their enormous support during field visits.

References

Abdullah AYM, Masrur A, Adnan MSG, Baky MdAA, Hassan QK, and Dewan A (2019) Spatio-temporal patterns of land use/land cover change in the heterogeneous coastal region of Bangladesh between 1990 and 2017. Remote Sens. 11:790. https://doi.org/10.3390/rs11070790

Adamu B, Tansey K, Ogutu B (2018) Remote sensing for detection and monitoring of vegetation affected by oil spills. Int J Remote Sens 39:3628–3645. https://doi.org/10.1080/01431161. 2018.1448483

Agbagwa IO, Ndukwu BC (2014) Oil and gas pipeline construction-induced forest fragmentation and biodiversity loss in the Niger Delta, Nigeria. Nat Resour 05:698–718. https://doi.org/10.4236/nr.2014.512061

Ahmed N, Howlader N, Hoque MA-A, Pradhan B (2021) Coastal erosion vulnerability assessment along the eastern coast of Bangladesh using geospatial techniques. Ocean Coast Manag 199:105408. https://doi.org/10.1016/j.ocecoaman.2020.105408

Aji MAP, Kamal M, Farda NM (2023) Mangrove species mapping through phenological analysis using random forest algorithm on Google Earth Engine. Remote Sens Appl 30:100978. https://doi.org/10.1016/j.rsase.2023.100978

Akhtar N, Tsuyuzaki S (2024) Effects of disturbances on the spatiotemporal patterns and dynamics of coastal wetland vegetation. Ecol Indic 166:112430. https://doi.org/10.1016/j.ecolind.2024.112430

Arshad M, Eid EM, Hasan M (2020) Mangrove health along the hyper-arid southern Red Sea coast of Saudi Arabia. Environ Monit Assess 192. https://doi.org/10.1007/s10661-020-8140-6

Aung TS, Overland I, Vakulchuk R, Xie Y (2022) The environmental burdens of special economic zones on the coastal and marine environment: A remote sensing assessment in Myanmar. Remote Sens Appl 28:100809. https://doi.org/10.1016/j.rsase.2022.100809

Avci C, Budak M, Yağmur N, Balçik F (2023) Comparison between random forest and support vector machine algorithms for LULC classification. Int J Eng Geosci 8:1–10. https://doi.org/10.26833/ijeg.987605

Barua P, Rahman SH (2019) Sustainable livelihood of vulnerable communities in southern coast of Bangladesh through the utilization of mangroves. Asian J Water Environ Pollut 16:59–67. https://doi.org/10.3233/ajw190007

Benfield SL, Guzman HM, Mair JM (2005) Temporal mangrove dynamics in relation to coastal development in Pacific Panama. J Environ Manag 76:263–276. https://doi.org/10.1016/j.jenvman.2005.02.004

BEZA (2014) Feasibility study for Mirershorai Economic Zone. Bangladesh Economic Zones Authority (BEZA), Government of the People's Republic of Bangladesh. https://beza.gov.bd/econo mic-zones-site/ .Accessed 04 November 2024

Bhattacharjee S, Islam MT, Kabir ME, Kabir MM (2021) Land-use and land-cover change detection in a north-eastern wetland ecosystem of Bangladesh using remote sensing and GIS techniques. Earth Syst Environ 5:319–340.https://doi.org/10.1007/s41748-021-00228-3

BMD (2023) Climate data portal. Bangladesh Meteorological Department (BMD). http://bmd.gov.bd. Accessed 02 November 2024

Brammer H (2013) Bangladesh's dynamic coastal regions and sea-level rise. Clim Risk Manag 1:51–62. https://doi.org/10.1016/j.crm.2013.10.001

Chow J (2018) Mangrove management for climate change adaptation and sustainable development in coastal zones. J Sustain For 37(2), 139– 156 https://doi.org/10.1080/10549811.2017.1339615

Chowdhury MShN, Hossain, Mitra A, Barua P (2022) Environmental functions of the Teknaf Peninsula mangroves of Bangladesh to communicate the values of goods and services.

Mesopotamian Journal of Marine Sciences 26:79–97. https://doi.org/10.58629/mjms.v26i1.193

Congedo L (2021) Semi-automatic classification plugin: A Python tool for the download and processing of remote sensing images in QGIS. Int J Open Source Softw 6:3172. https://doi.org/10.21105/joss.03172

Craft C (2022) Creating and restoring wetlands from theory to practice. Elsevier, Amsterdam, Netherlands

Daigle P (2010) A summary of the environmental impacts of roads, management responses, and research gaps: A literature review. J Ecosyst Manag 10(3). https://doi.org/10.22230/jem.2010v10n3a38

Din N, Ngo-Massou VM, Essomè-Koum GL, Ndema-Nsombo E, Kottè-Mapoko E, Nyamsi-Moussian L (2017) Impact of urbanization on the evolution of mangrove ecosystems in the Wouri River Estuary (Douala Cameroon). In C. W. Finkl and C. Makowski (Eds.), Coastal wetlands: alteration and remediation (Vol. 21, pp. 81–131). Springer International Publishing. https://doi.org/10.1007/978-3-319-56179-0_3

Ellis JT, Spruce JP, Swann RA, Smoot JC, Hilbert KW (2011) An assessment of coastal land-use and land-cover change from 1974–2008 in the vicinity of Mobile Bay, Alabama. J Coast Conserv 15(1):139–149.https://doi.org/10.1007/s11852-010-0127-y

Fan B, Li Y, Zhang Z, Yang Y, Li Y (2024) Exploring cumulative vulnerability of mangrove forests to intensive coastal anthropogenic threats. Ecosyst Health Sustain 10. https://doi.org/10.34133/ehs.0153

FAO (2020) Global Forest Resources Assessment 2020: Main report. Rome.https://doi.org/10.4060/ca9825en

Farr TG., Rosen P A, Caro E, Crippen R, Duren R, Hensley S, et al. (2007). The shuttle radar topography mission. Rev Geophys 45:. https://doi.org/10.1029/2005rg000183

Ghosh M, Kumar L, Roy C (2016) Mapping long-term changes in mangrove species composition and distribution in the Sundarbans. Forests 7:305. https://doi.org/10.3390/f7120305

Gilman E L, Ellison J, Duke N C & Field C (2008) Threats to mangroves from climate change and adaptation options: A review. Aquatic Botany, 89(2), 237–250. https://doi.org/10.1016/j.aquabot.2007.12.009

Gorelick N, Hancher M, Dixon M, Ilyushchenko S, Thau D, Moore R (2017) Google Earth Engine: planetary-scale geospatial analysis for everyone. Remote Sens Environ 202:18–27. https://doi.org/10.1016/j.rse.2017.06.031

Hasan M, Hassan L, Al MA, Kamal AHM, Idris MH, Hoque MZ, Mahmoood R, Alam MN, Ali A (2024) Human intervention caused massive destruction of the second largest mangrove forest, Chakaria Sundarbans, Bangladesh. Environ Sci Pollut Res 31: 25329–25341. https://doi.org/10.1007/s11356-024-32792-2

Hayashi SN, Souza-Filho PWM, Nascimento WR, Fernandes MEB (2019) The effect of anthropogenic drivers on spatial patterns of mangrove land use on the Amazon coast. PLoS ONE 14:e0217754. https://doi.org/10.1371/journal.pone.0217754

He NH, Garcia EA (2009) Learning from imbalanced data. IEEE Trans Knowl Data Eng 21:1263–1284. https://doi.org/10.1109/tkde.2008.239

Hoque MZ, Cui S, Islam I, Xu L, Tang J (2020) Future impact of land use/land cover changes on ecosystem services in the lower Meghna river estuary, Bangladesh. Sustainability 12:2112. https://doi.org/10.3390/su12052112

Hoque MZ, Cui S, Islam I, Xu L, Ding S (2021) Dynamics of plantation forest development and ecosystem carbon storage change in coastal Bangladesh. Ecol Indic 130:107954. https://doi.org/10.1016/j.ecolind.2021.107954

Hoque ZM, Islam I, Ahmed M, Hasan SS, Prodhan AF (2022) Spatio-temporal changes of land use land cover and ecosystem service values in coastal Bangladesh. Egypt J Remote Sens Space Sci 25:173–180. https://doi.org/10.1016/j.ejrs.2022.01.008

Huete AR (1988) A soil-adjusted vegetation index (SAVI). Remote Sens Environ 25:295–309. https://doi.org/10.1016/0034-4257(88)90106-x

Huete A, Didan K, Miura T, et al (2002) Overview of the radiometric and biophysical performance of the MODIS vegetation indices. Remote Sens Environ 83:195–213. https://doi.org/10.1016/s0034-4257(02)00096-2

Islam K, Jasim UM, Nath B, Nath TK (2016) Quantitative assessment of land cover change using Landsat time series data: case of Chunati Wildlife Sanctuary (CWS), Bangladesh. Int J Envir Geoform 3:45–55. https://doi.org/10.30897/ijegeo.306471

Islam MdM, Borgqvist H, Kumar L (2019) Monitoring mangrove forest landcover changes in the coastline of Bangladesh from 1976 to 2015. Geocarto Int 34:1458–1476. https://doi.org/10.1080/10106049.2018.1489423

Islam I, Cui S, Hoque MZ, Abdullah HM, Tonny KF, Ahmed M, Ferdush J, Xu L, and Ding S (2022) Dynamics of Tree outside Forest Land Cover Development and Ecosystem Carbon Storage Change in Eastern Coastal Zone, Bangladesh. Land, 11(1):76. https://doi.org/10.3390/land11010076

Jia M, Wang Z, Mao D, et al (2023) Mapping global distribution of mangrove forests at 10-m resolution. Sci Bull 68:1306–1316. https://doi.org/10.1016/j.scib.2023.05.004

Jiang Z, Huete AR, Didan K, Miura T (2008) Development of a two-band enhanced vegetation index without a blue band. Remote Sens Environ 112:3833–3845. https://doi.org/10.1016/j.rse.2008.06.006

Kadri N, Jebari S, Augusseau X, Mahdhi N, Lestrelin G, Berndtsson R (2023) Analysis of four decades of land use and land cover change in semiarid Tunisia using google earth engine. Remote Sens 15:3257. https://doi.org/10.3390/rs15133257

Kelly JT, Gontz AM (2017) Using GPS-surveyed intertidal zones to determine the validity of shorelines automatically mapped by Landsat water indices. Int J Appl Earth Obs Geoinf 65:92–104. https://doi.org/10.1016/j.jag.2017.10.007

Kirui KB, Kairo JG, Bosire J, Viergever KM, Rudra S, Huxham M, and Briers RA (2011) Mapping of mangrove forest land cover change along the Kenya coastline using Landsat imagery. Ocean Coast Manag 83: 19–24. https://doi.org/10.1016/j.ocecoaman.2011.12.004

Kirwan ML, Megonigal JP (2013) Tidal wetland stability in the face of human impacts and sea-level rise. Nature 504:53–60. https://doi.org/10.1038/nature12856

Kouassi CJA, Qian C, Khan D, Achille LS, Kebin Z, Omifolaji JK, Yang X (2023) Google Earth Engine for Landsat image processing and assessing LULC classification in southwestern Côte D’ivoire. Geod Cartogr 49:37–50. https://doi.org/10.3846/gac.2023.16805

Li W, Dong R, Fu H, Wang J, Yu L,Gong P (2019) Integrating Google Earth imagery with Landsat data to improve 30-m resolution land cover mapping. Remote Sens Environ 237:111563. https://doi.org/10.1016/j.rse.2019.111563

Long K, Chen Z, Zhang H, Zhang M (2023) Spatiotemporal disturbances and attribution analysis of mangrove in southern China from 1986 to 2020 based on time-series Landsat imagery. Sci Total Environ 912:169157. https://doi.org/10.1016/j.scitotenv.2023.169157

Loulad S, Nguyen TT, Simou MR, Rhinane H, Buerkert A (2023) Monitoring rural-urban transformation in the coastal region of Rabat-Sale-Kenitra, Morocco. PLoS ONE 18:e0290829. https://doi.org/10.1371/journal.pone.0290829

Martín EG, Costa MM, Máñez KS (2020) An operationalized classification of nature based solutions for water-related hazards: from theory to practice. Ecol Econ 167:106460. https://doi.org/10.1016/j.ecolecon.2019.106460

Maryantika N, Lin C (2017) Exploring changes of land use and mangrove distribution in the economic area of Sidoarjo District, East Java using multi-temporal Landsat images. Inf Process Agric 4:321–332. https://doi.org/10.1016/j.inpa.2017.06.003

McConchie D, Saenger P (1991) Mangrove forests as an alternative to civil engineering works in coastal environments of Bangladesh: lessons for Australia. In Proceedings of 1990 workshop on coastal zone management (pp. 220-233). Geo-Processors Pty Ltd.

McHugh ML (2012) Interrater reliability: the kappa statistic. Biochem Med 276–282. https://doi.org/10.11613/bm.2012.031

Miah MT, Fariha JN, Kafy AA, Islam R, Biswas N, Duti BM, Fattah Md A, Alsulamy S, Khedher KM, and Salem MA (2024) Exploring the nexus between land cover change dynamics and spatial heterogeneity of demographic trajectories in rapidly growing ecosystems of south Asian cities. Ecol Indic 158: 111299. https://doi.org/10.1016/j.ecolind.2023.111299

Midekisa A, Holl F, Savory DJ, et al (2017) Mapping land cover change over continental Africa using Landsat and Google Earth Engine cloud computing. PLoS ONE 12:e0184926. https://doi.org/10.1371/journal.pone.0184926

Nabila IA, Tsuyuzaki S (2025) Examining the effects of economic zone construction on mangrove forest using Before-After-Control-Impact (BACI). Environ Monit Assess, 197:949, https://doi.org/10.1007/s10661-025-14380-0

Nasiri V, Deljouei A, Moradi F, Sadeghi SMM, Borz SA (2022) Land use and land cover mapping using Sentinel-2, Landsat-8 satellite images, and Google Earth Engine: a comparison of two composition methods. Remote Sens 14:1977. https://doi.org/10.3390/rs14091977

Naskar M, Blinnikov M, Ghosh R, Das S, Paruya D K, Majumdar S, and Bera S (2021) A diagnostic phytolith morphotype found in Porteresia coarctata (Roxb.) Tateoka indicates coastal swampy mangrove environments: A case study from the Indian east coast. Flora 282:151884. https://doi.org/10.1016/j.flora.2021.151884

Otero V, Quisthoudt K, Koedam N, Dahdouh-Guebas F (2016) Mangroves at their limits: detection and area estimation of mangroves along the Sahara desert coast. Remote Sens 8:512. https://doi.org/10.3390/rs8060512

Patil A, Panhalkar S (2023) Comparative analysis of machine learning algorithms for land use and land cover classification using Google Earth Engine platform. J Geomat 17:111–118. https://doi.org/10.58825/jog.2023.17.2.96

Peel MC, Finlayson BL, McMahon TA (2007) Updated world map of the Köppen-Geiger climate classification. Hydrol Earth Syst Sci 11:1633–1644. https://doi.org/10.5194/hess-11-1633-2007

Phan TN, Kuch V, Lehnert LW (2020) Land cover classification using Google Earth Engine and random forest classifier-the role of image composition. Remote Sens 12:2411. https://doi.org/10.3390/rs12152411

Purwanto N, Latifah S, Yonariza N, Akhsani F, Sofiana EI, Ferdiansah MR (2023) Land cover change assessment using random forest and CA markov from remote sensing images in the protected forest of South Malang, Indonesia. Remote Sens Appl 32:101061. https://doi.org/10.1016/j.rsase.2023.101061

Rahman M M, Jiang Y & Irvine K (2018) Assessing wetland services for improved development decision-making: a case study of mangroves in coastal Bangladesh. Wetl. Ecol. Manag. 26(4), 563–580. https://doi.org/10.1007/s11273-018-9592-0

Ramezan CA, Warner TA, Maxwell AE, Price BS (2021) Effects of training set size on supervised machine-learning land-cover classification of large-area high-resolution remotely sensed data. Remote Sens 13:368. https://doi.org/10.3390/rs13030368

Richards DR, Friess DA (2016) Rates and drivers of mangrove deforestation in Southeast Asia, 2000–2012. Proceedings of the National Academy of Sciences of the United States of America, 113(2): 344–349. https://doi.org/10.1073/pnas.1510272113

Romañach SS, DeAngelis DL, Koh HL, et al (2018) Conservation and restoration of mangroves: global status, perspectives, and prognosis. Ocean Coast Manag 154:72–82. https://doi.org/10.1016/j.ocecoaman.2018.01.009

Roy SS, Ghosh T, Hewavithana DK (2024) Transformation of coastal wetlands in the Sundarban delta (1999–2020). Environ Monit Assess 196:. https://doi.org/10.1007/s10661-024-12901-x

Saenger P, Siddiqi NA (1993) Land from the sea - The Mangrove afforestation program of Bangladesh. Ocean Coast Manage 20 (1): 23–39 https://doi.org/10.1016/0964-5691(93)90011-M

Shawul AA, Chakma S (2019) Spatiotemporal detection of land use/land cover change in the large basin using integrated approaches of remote sensing and GIS in the Upper Awash basin, Ethiopia. Environ Earth Sci 78:. https://doi.org/10.1007/s12665-019-8154-y

Sosnovskikh S (2017) Industrial clusters in Russia: the development of special economic zones and industrial parks. Russ J Econ 3:174–199. https://doi.org/10.1016/j.ruje.2017.06.004

SRDI (2010) Saline Soils of Bangladesh. Soil Resource Development Institute (SRDI), SRMAF project, Ministry of Agriculture, Government of the People's Republic of Bangladesh.https://srdi.portal.gov.bd/sites/default/files/files/srdi.portal.gov.bd/publications/bc598e7a_df21_49ee_882e_0302c974015f/Soil%20salinity%20report-Nov%202010.pdf

Suratman MN (2008) Carbon sequestration potential of mangroves in Southeast Asia. In Bravo F,Jandl R, LeMay V, Von Gadow K (eds.), Managing forest ecosystems: The challenge of climate change. managing forest ecosystems. Springer, Dordrecht 17: 297-315. https://doi.org/10.1007/978-1-4020-8343-3_17

Taillardat P, Friess D A, & Lupascu M (2018) Mangrove blue carbon strategies for climate change mitigation are most effective at the national scale. Biol Lett, *14*(10), 20180251. https://doi.org/10.1098/rsbl.2018.0251

Tang K (2022) The political economy of special economic zones: the cases of Ethiopia and Vietnam. Rev Int Political Econ 30(5), 1957–1983. https://doi.org/10.1080/09692290.2022.2152073

Tesfaye W, Elias E, Warkineh B, et al (2024) Modeling of land use and land cover changes using Google Earth Engine and machine learning approach: implications for landscape management. Environ Syst Res 13:.https://doi.org/10.1186/s40068-024-00366-3

Tewabe D, Fentahun T (2020) Assessing land use and land cover change detection using remote sensing in the Lake Tana Basin, Northwest Ethiopia. Cogent Environmental Science, 6(1) https://doi.org/10.1080/23311843.2020.1778998

Thomas N, Lucas R, Bunting P, Hardy A, Rosenqvist A, and Simard M (2017) Distribution and drivers of global mangrove forest change, 1996–2010. PLoS ONE 12(6):1996–2010. https://doi.org/10.1371/journal.pone.017930

Tucker CJ (1979) Red and photographic infrared linear combinations for monitoring vegetation. Remote Sens Environ 8:127–150. https://doi.org/10.1016/0034-4257(79)90013-0

Uddin MM, Rahman MdS, Hossain MK, Akter S (2014) Growth density and regeneration of afforested mangroves at Mirersarai forest range in Bangladesh. Forest Sci Technol 10:120–124. https://doi.org/10.1080/21580103.2013.874375

Uddin MM, Hossain MM, Aziz AA, Lovelock CE (2022) Ecological development of mangrove plantations in the Bangladesh delta. For Ecol Manag 517:120269. https://doi.org/10.1016/j.foreco.2022.120269

Ullah MH, Mondal MAI, Uddin MR, Ferdous MA (2010) Implications of mangrove wetland in socio-environmental sector: experiences from southeast coast of Chittagong, Bangladesh. J Forest Environ Sci 26:103–111 https://doi.org/10.7747/JFS.2010.26.2.103

Van Vliet J (2019) Direct and indirect loss of natural area from urban expansion. Nat Sustain 2:755–763. https://doi.org/10.1038/s41893-019-0340-0

Waleed M, Sajjad M, and Shazil MS (2024) Urbanization-led land cover change impacts terrestrial carbon storage capacity: A high-resolution remote sensing-based nation-wide assessment in Pakistan (1990–2020). Environ Impact Assess Rev 105: 107396. https://doi.org/10.1016/j.eiar.2023.107396

Xu H (2006) Modification of normalised difference water index (NDWI) to enhance open water features in remotely sensed imagery. Int J Remote Sens 27:3025–3033. https://doi.org/10.1080/01431160600589179

Yuh YG, Tracz W, Matthews HD, Turner SE (2022) Application of machine learning approaches for land cover monitoring in northern Cameroon. Ecol Inform 74:101955. https://doi.org/10.1016/j.ecoinf.2022.101955

812

Supplementary Information

Assessing land use and land cover changes from 1989 to 2021 in relation to economic zone construction along mangrove forests on the east coast of Bangladesh

Journal name

Journal of Coastal Conservation

Author names, affiliation and e-mail address of the corresponding author

Irtifa Alam Nabila [1,2], Shiro Tsuyuzaki[3]

[1]Graduate School of Environmental Science, Hokkaido University, Sapporo 060-0810, Hokkaido, Japan

[2]Department of Geography and Environment, Jahangirnagar University, Savar, Dhaka 1342, Bangladesh

[3]Graduate School of Environmental Earth Science, Hokkaido University, Sapporo 060-0810, Hokkaido, Japan

Correspondence

Irtifa Alam Nabila

Email: irtifaalam.nabila.m4@elms.hokudai.ac.jp

Table S1 Confusion matrices showing misclassification among LULC types and classification accuracy from 2001 to 2021

LULC	2001									
	Agricultural land	Homestead vegetation	Artificial water	Grassland	Forest	Bare land	Mudflat	Seawater	Total	User accuracy (%)
Agricultural land	19	1	0	1	0	4	0	0	25	76
Homestead vegetation	1	156	3	4	32	0	0	2	198	79
Artificial water	0	4	14	4	1	0	0	2	25	56
Grassland	3	13	1	53	6	0	8	3	87	61
Forest	0	66	0	3	192	0	0	0	261	74
Bare land	1	0	0	1	0	34	0	0	36	94
Mudflat	0	0	1	11	0	0	73	2	87	84
Seawater	0	0	7	2	0	0	0	59	68	87
Total	24	240	26	79	231	38	81	68	787	
Producer accuracy (%)	79	65	54	67	83	89	90	87		

LULC	2011									
	Agricultural land	Homestead vegetation	Artificial water	Grassland	Forest	Bare land	Mudflat	Seawater	Total	User accuracy (%)
Agricultural land	23	0	0	0	0	3	0	0	26	88
Homestead vegetation	1	90	3	1	52	0	0	1	148	61
Artificial water	0	5	20	0	0	0	2	4	31	65
Grassland	3	1	0	46	2	4	14	0	70	66
Forest	0	27	0	4	292	0	1	0	324	90
Bare land	5	0	0	2	1	14	0	0	22	64
Mudflat	0	0	0	9	1	0	60	1	71	85
Seawater	0	0	4	2	0	0	7	53	66	80
Total	32	123	27	64	348	21	84	59	758	
Producer accuracy (%)	72	73	74	72	84	67	71	90		

LULC	2014									
	Agricultural land	Homestead vegetation	Artificial water	Grassland	Forest	Bare land	Mudflat	Seawater	Total	User Accuracy (%)
Agricultural land	30	3	0	0	0	2	0	0	35	86
Homestead vegetation	5	108	1	3	26	1	1	0	145	74
Artificial water	0	0	25	2	1	0	1	2	31	81
Grassland	0	1	0	51	2	1	5	0	60	85
Forest	1	24	0	8	224	0	0	0	257	87
Bare land	0	0	0	3	1	8	0	0	12	67
Mudflat	0	0	0	5	0	0	58	0	63	92
Seawater	0	3	0	2	0	0	4	64	73	88
Total	36	139	26	74	254	12	69	66	676	
Producer Accuracy (%)	83	78	96	69	88	67	84	97		

LULC	2021										
	Built-up land	Agricultural land	Homestead vegetation	Artificial water	Grassland	Forest	Bare land	Mudflat	Seawater	Total	User accuracy (%)
Built-up land	72	1	0	0	0	0	1	0	0	74	97
Agricultural land	0	64	1	0	11	0	14	0	0	90	71
Homestead vegetation	0	5	74	0	1	34	4	0	0	118	63
Artificial water	0	0	0	74	0	0	0	9	5	88	84
Grassland	0	10	2	0	33	3	8	2	0	58	57
Forest	0	0	20	0	2	268	0	0	0	290	92
Bare land	1	8	5	0	1	0	35	0	0	50	70
Mudflat	2	0	0	1	0	0	0	32	5	40	80
Seawater	0	0	0	5	0	0	0	4	58	67	87
Total	75	88	102	80	48	305	62	47	68	800	
Producer accuracy (%)	96	73	73	93	69	88	56	68	85		

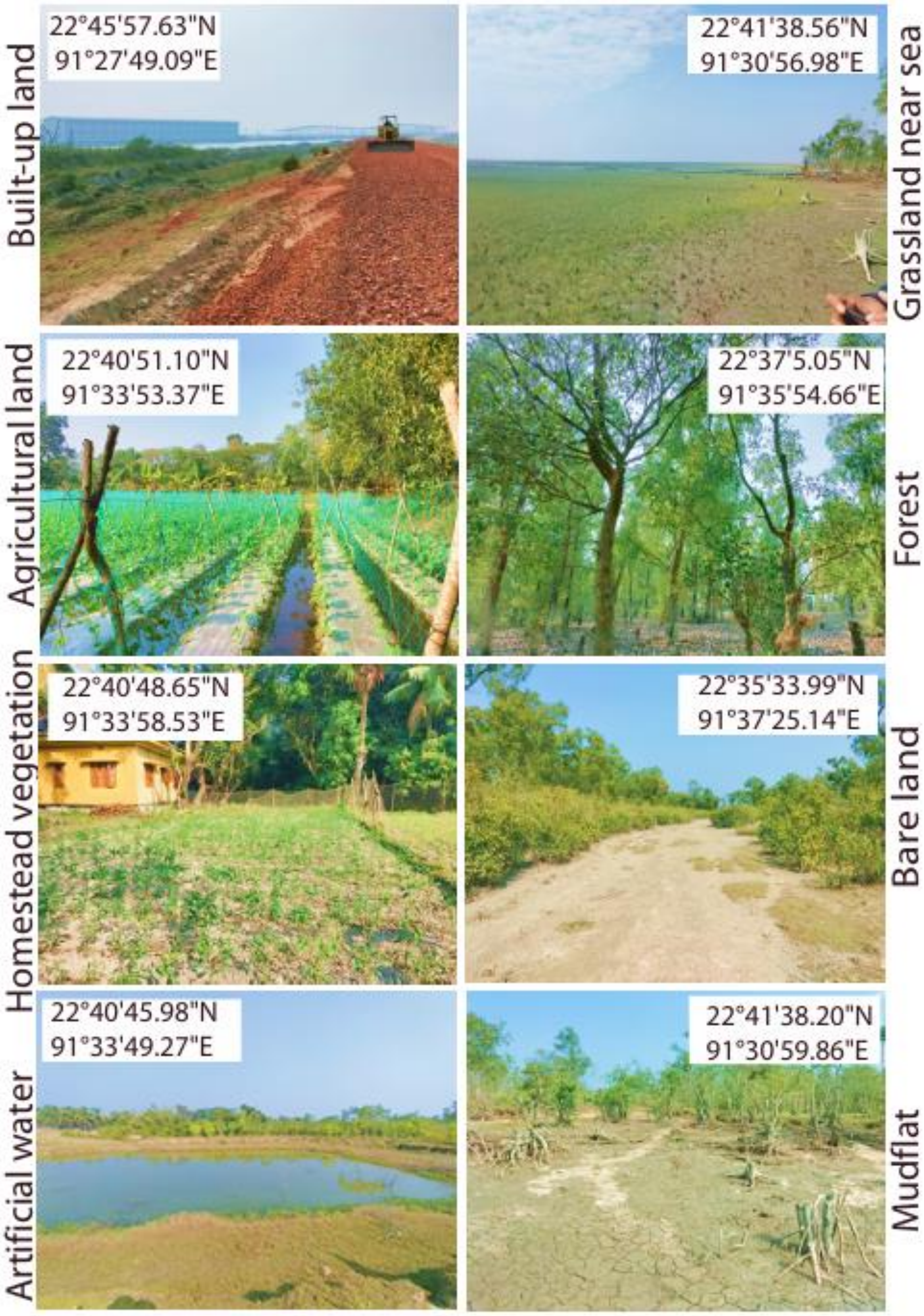

Fig. S1 LULC types recorded with geographic coordinates in November 2021.